Spot profile analysis and lifetime mapping in ultrafast electron diffraction: Lattice excitation of self-organized Ge nanostructures on Si(001)

T. Frigge,[a] B. Hafke, V. Tinnemann,[b] T. Witte, and M. Horn-von Hoegen
Department of Physics and Center for Nanointegration (CENIDE), University of Duisburg-Essen, Lotharstr. 1, 47057 Duisburg, Germany

(Received 24 April 2015; accepted 22 May 2015; published online 5 June 2015)

Ultrafast high energy electron diffraction in reflection geometry is employed to study the structural dynamics of self-organized Germanium hut-, dome-, and relaxed clusters on Si(001) upon femtosecond laser excitation. Utilizing the difference in size and strain state the response of hut- and dome clusters can be distinguished by a transient spot profile analysis. Surface diffraction from {105}-type facets provide exclusive information on hut clusters. A pixel-by-pixel analysis of the dynamics of the entire diffraction pattern gives time constants of 40, 160, and 390 ps, which are assigned to the cooling time constants for hut-, dome-, and relaxed clusters.
[http://dx.doi.org/10.1063/1.4922023]

I. INTRODUCTION

The ultrafast structural dynamics of impulsively excited non-equilibrium processes at surfaces and in solids have recently attracted much attention. Utilizing diffraction at Ångström wavelength facilitates insight into structural changes on a picometer spatial dimension and thus has opened a window to an undiscovered science. Ultrafast time-resolved diffraction experiments were enabled by the availability of laser systems providing intense femtosecond pulses and triggered by the limitations of ultrafast spectroscopy as a structural probe. Based on plasma generated X-ray pulses[1–4] or photo excited electron pulses,[5–9] a temporal resolution in the femtosecond regime became possible. The ultrafast motion of atoms upon excitation was directly determined from the transient change of diffraction spot intensity.[10–12] New states of matter were observed through changes of fundamental material properties like bond hardening or softening.[13,14]

The observation of ultrafast structural dynamics at surfaces or in nanostructures supported by a solid substrate, however, is not possible with X-rays but requires the orders of magnitude higher scattering cross section of electrons with matter. Low energy electron diffraction (LEED) or reflection high energy electron diffraction (RHEED) provides superior surface sensitivity, i.e., they are ideally suited to probe surfaces or ultrasmall epitaxial structures. Due to the high scattering cross section, the penetration depth beneath the surface is of the order of a few Ångström only, in both cases.[15]

The structural and morphological features of a surface or of epitaxial nanostructures are all reflected in the spots and features of a LEED or RHEED diffraction pattern. From the spot distance in reciprocal space, the lattice parameter a_0 and strain state of the sample is directly determined. The width of the spots is reciprocally proportional to the size of the diffracting nanostructures. The Debye-Waller effect describes how thermal motion of the atoms causes reduction of the spot intensity and results in an increase of diffuse intensity of the

[a]Electronic mail: tim.frigge@uni-due.de.
[b]Present address: Leibniz Institute for New Materials (INM), 66123 Saarbrücken, Germany.

background.[16] In a time-resolved electron diffraction experiment, we can employ all these diffraction features at the same time to distinguish how different processes evolve on different timescales after excitation.

The required temporal resolution in the pico- or femtosecond regime is obtained through a pump probe setup. The sample is excited by an ultrashort femtosecond laser pulse (pump). The transient evolution of the excitation and relaxation processes is determined by diffraction from a time delayed electron pulse (probe). The demand for surface sensitivity in combination with a high temporal resolution makes the use of high energy electrons under gracing incidence the versatile tool for time-resolved surface science.[17–20] In a recent work, Gulde *et al*. demonstrated that also picosecond pulses of low energy electrons can be employed to resolve the structural dynamics in a single polymer layer supported by graphene in transmission geometry.[21]

In this paper, we will employ nanoscale heat transport from Germanium (Ge) nanoclusters into a Silicon (Si) substrate[22] to demonstrate the capabilities of time-resolved electron diffraction to observe different transient processes in parallel from the same diffraction experiment. The standard techniques for the determination of the transient temperature evolution of thin films are ultrafast optical methods like time-domain thermoreflectance (TDTR).[23,24] Due to the low scattering cross section of light with matter, they are, however, usually restricted to thicker films. Furthermore, the measured transient change of reflectivity is an integral response of the entire probed sample surface. Thus, it is not possible to distinguish between the transient response of different nanoscale structures, e.g., self-organized clusters of different dimensions which may simultaneously be present at the sample. Here, we demonstrate in detail how time-resolved electron diffraction can be used to distinguish between the transient contributions from three different cluster types upon impulsive excitation by an intense fs laser pulse. The change of temperature upon laser induced heating can be observed by the transient drop of spot intensity in the diffraction pattern, as described by the Debye-Waller effect. A spot profile analysis of the diffraction spots allows to unambiguously distinguish between the cooling rates of the three different cluster types. The self-organized growth of Ge on Si(001) was utilized to prepare a sample with well defined epitaxial hut-, dome- and relaxed Ge clusters.

A. Growth of Ge/Si(001)

Epitaxial Ge nanostructures on Si(001) were used as a model system. Both materials crystallize in cubic diamond structure. They exhibit a lattice mismatch of 4.2% (at room temperature) which prevents the Frank-van der Merwe type growth of smooth Germanium layers on Silicon.[25] At typical growth temperatures between 400 °C and 700 °C, islanding is observed after the formation of a thin wetting layer, i.e., the so-called Stranski-Krastanov growth mode. Initially, a pseudomorphous Ge film grows in a layer-by-layer fashion with the lattice constant of the underlying Si substrate. The strain energy increases with film thickness. This wetting layer becomes unstable for thicknesses of more than three monolayers of Ge (1ML = 6.24 $\times 10^{14}$ atoms/cm^2). With increasing coverage, the formation of a metastable phase, so-called hut clusters, is observed, which are explained as a first step on the kinetic pathway from layer-by-layer growth to islanding.[26,27,29]

Hut clusters are composed of four {105}-type facets, which form an angle of 11.3° with the {001} Si substrate surface plane. This leads to a rectangular or square shape, as sketched in Fig. 1. Typical dimensions are 23 nm width at a height of only 2.3 nm.[28,29] As soon as the whole surface is covered with hut clusters, which should typically be the case after about 6 ML—a transformation to the next step larger islands is observed.[30–32] The formation of steeper facets allows for a more efficient reduction of lattice mismatch induced strain than in the case of huts.[32–34] With respect to their special shape, these larger clusters are usually denoted as dome clusters. Due to their complex faceting structure, their base area exhibits an approximately round shape with a diameter of 50–60 nm at a height of 5–6 nm, as sketched in Fig. 1. Both cluster types are free of lattice mismatch relieving defects and dislocations.[35,36] The build-up of strain and the subsequent strain relief by islanding is the driving force for

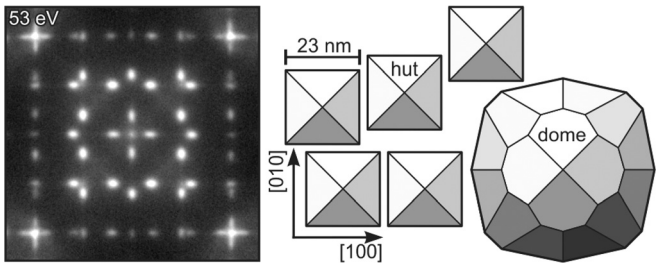

FIG. 1. Illustration of the two different cluster types: hut clusters, composed of four {105}-type facets and larger dome clusters with a complex faceting. The LEED pattern reflects the diffraction from the four {105}-type facets of the hut clusters.

this self-organized and kinetically self-limited formation of clusters. For this reason their size distribution is very narrow.[36–39]

The strain is reduced during the different transition states from layers to huts and then to domes. For hut clusters, the strain relief is about 15%–20%. Thus, the hut clusters are still lateral compressed and the vertical layer distance is significantly expanded by tetragonal distortion.[32,35] In the case of dome clusters, Cerullo showed that a large part of the strain is compensated through elastic deformation of the substrate.[36] Relaxation towards the Ge bulk lattice constant is thus more efficient for the dome clusters.[40] Finally, the generation of defects and dislocations accommodates the lattice mismatch and causes the formation of large and fully relaxed 3D islands. Such islands do not grow any longer in a self-organized and kinetically self-limited way. As a consequence, those relaxed clusters exhibit a very broad size distribution.[36,41]

II. EXPERIMENTAL

The experimental setup of the laser system in combination with the electron diffraction is sketched in Fig. 2. A regenerative 5 kHz Ti:Sapphire system provides intense 50 fs laser pulses with 200 μJ pulse energy at a wavelength of 800 nm. The initial beam is split into two parts by a T80:R20 beam splitter. The more intensive beam is used to excite the sample surface under normal incidence (pump). The excitation fluence could be adjusted between 0.1 mJ/cm^2 and 8 mJ/cm^2. The lower intensity beam is frequency tripled to a photon energy of 4.55 eV. These pulses are then used to generate ultrashort electron bunches by single photon emission from a back illuminated 10 nm thin Au photocathode. The electron bunches are subsequently accelerated to 20 keV in a high extraction field of 5.0 kV/mm (probe). The grazing angle of incidence of 3° to 5° ensures the high surface sensitivity of the electrons in the RHEED experiment. Diffraction patterns are image intensified by a combination of a microchannelplate (MCP) and a phosphor screen. The pattern is recorded by a cooled CCD camera.[17,18,42]

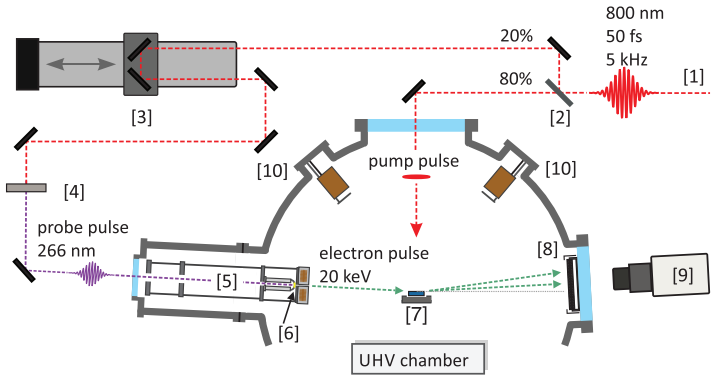

FIG. 2. Sketch of the time-resolved RHEED setup. (1) reg. amplifier, (2) T80:R20 beam splitter, (3) optical delay line 50 cm (–300 ps–3000 ps), (4) BBOs, (5) electron gun, (6) Au photocathode and extraction field, (7) sample (25 K to 1600 K), (8) MCP and phosphor screen, (9) cooled CCD-camera, and (10) evaporators.

Finally, a movie of transient diffraction patterns is obtained by the systematic variation of the time delay between the laser pump pulse and the electron probe pulse through a 50 cm optical delay line (−300 ps to 3000 ps). In order to enhance the signal to noise ratio, each diffraction pattern is averaged over 60 single frames, each one recorded at an exposure time of 200 ms. The influence of low frequency pointing instability and intensity variations of the laser beam during the course of an experiment was eliminated by the alternating use of a shutter in the beam path of the pump pulse. Thus, each diffraction pattern was normalized to a corresponding one without excitation.

The sample preparation and all measurements are performed under ultra-high vacuum conditions (UHV) at a base pressure of $p < 10^{-10}$ mbar. The UHV chamber is equipped with two evaporators for *in-situ* film growth and sample preparation. LEED is used to check the substrate prior to and after sample preparation as shown on the left side of Fig. 1. The sample can be cooled through a liquid He-cryostat to 25 K and heated by direct current up to 1600 K.

Prior to film preparation, the Si(001) sample was degassed for several hours and then flash annealed close to the melting point of 1414 °C. Germanium was deposited from a home build e-beam evaporator via molecular beam epitaxy (MBE). Prior to all experiments, the Ge flux of this evaporator was calibrated through LEED layer-by-layer oscillations during the surfactant mediated epitaxy of Ge on Si(111).[43] Finally, the sample was prepared by deposition of 8 ML Ge on a clean Si(001) surface at a temperature of 550 °C. After the experiment, the prepared Ge clusters were characterized *ex-situ* by atomic force microscopy (AFM).

III. RESULTS AND DISCUSSION

A. Composition of the diffraction pattern

Figure 3(a) shows the RHEED diffraction pattern of the initial bare Si(001) surface prior to deposition. The symmetry directions of the reciprocal space are shown in the lower right corner of the figure. The pattern was recorded at an electron energy of 20 keV and a sample temperature of 300 K. Electrons were incident along the [110] direction. The grazing incidence of the electrons leads to a vertical penetration depth of less than 1 nm. Considering surface diffraction, the periodicity of the reciprocal lattice perpendicular to the surface is lifted. In that case, the reciprocal lattice is described by a periodic arrangement of vertical lattice rods. The Laue condition is then satisfied for every intersection of the Ewald sphere and the rods of reciprocal lattice. This leads to a circular arrangement of spots. These circles, which are commonly known as *Laue zones* or *Laue circles*, are numbered in ascending order. Here, a series of intense spots show up located on the zero order Laue circle, i.e., clear indication for diffraction from an atomically flat, single crystalline surface. From the radius of the zero order Laue circle, a grazing angle of incidence of the electrons $\alpha \approx 3.2°$ is determined.

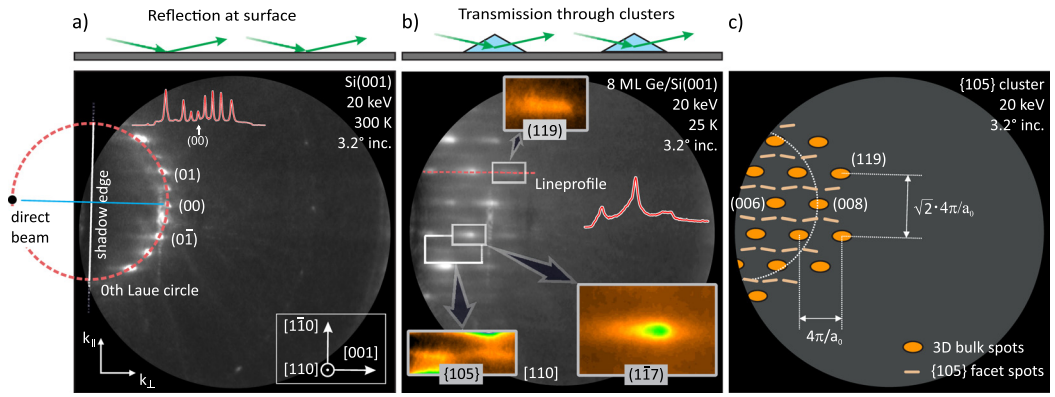

FIG. 3. Electron diffraction patterns of (a) the bare Si(001) surface prior to deposition and (b) after deposition of 8 ML Ge, grown at 550 °C. The diffraction geometry was in both cases the same, i.e., the incidence angle was 3.2° at an electron energy of 20 keV. Fig. (c) shows a schematic diffraction pattern of a surface covered with {105} faceted hut clusters under the same diffraction conditions. The presence of regularly ordered spots instead of a circular arrangement indicates that the diffraction happens in transmission.

After deposition of 8 ML of Ge, a sample with a high coverage of hut clusters ($8 \times 10^{10}\,\mathrm{cm}^{-2}$) and dome clusters ($2 \times 10^{9}\,\mathrm{cm}^{-2}$) was prepared. The change of morphology directly affects the electron diffraction pattern, as can be seen in Fig. 3(b). The typical circular arrangement of the spots for reflective diffraction from a flat surface has changed into a periodic ordered arrangement of equidistant spots which is indicative for diffraction in transmission geometry from single crystalline and epitaxial structures. This is in contrast to observations of Debye-Scherrer rings arising from diffraction from disordered, polycrystalline nanoparticles.[8] Because the grazing angle of incidence of the electrons of 3.2° is much lower than the hut cluster facet angle of 11.3°, electrons cannot be diffracted in reflection geometry from the {105} facets with orientations along the incident electron beam. Instead, they have undergone diffraction in transmission through the clusters. Thus, the diffraction pattern is described by a cut through a reciprocal diamond lattice in [001] direction. As depicted in the schematic diffraction pattern in Fig. 3(c), the distance of the spots is then given by $4\pi/a_0$ in [001] direction and in $[1\bar{1}0]$ direction by $\sqrt{2} \cdot 4\pi/a_0$, respectively, and a_0 the size of the cubic unit cell.

With the knowledge of the position of the (00) spot of the Si(001) substrate (see Fig. 3(a)) and the grazing angle of incidence of 3.2°, we can assign each spot to a Bragg reflection for a diamond lattice. Kinematically forbidden spots are described in terms of double diffraction, which is a prevalent effect in RHEED.[44,45] Fig. 3(c) also shows the original position of the zero order Laue circle. Thus all Bragg reflections in the vicinity of this circle have a very low distance to the Ewald sphere and hence the corresponding spots exhibit a high diffraction intensity which is clearly visible in Fig. 3(b).

In addition to the transmission spots, we also expect reflection spots from those {105} facets oriented perpendicular to the incident electron beam as reported by Aumann *et al.*[46] Each of the transmission spots is then accompanied by four {105} facet surface diffraction spots facing towards the transmission spot. These facet spots are located between the transmission spots and can clearly be identified in the contrast enhanced inset of Fig. 3(b).

In order to distinguish the contributions from the different cluster types to the diffraction pattern, we applied spot profile analysis. Figure 4 depicts a line-profile along the marked red line in Fig. 3(b). The intensity is plotted as function of $k_\perp$ along the direction through the (117) and the (119) spot. The experimental data can be described by a pair of two Gaussians of different widths, positions, and intensities. The broadening and shift of spots is explained in terms of different size and strain state of the huts, domes, and relaxed clusters as is schematically depicted in Fig. 5.

During diffraction, the finite size of the clusters effectively acts as a slit with finite width, i.e., the height, width, and length of the clusters. Thus, the diffraction spots of the smallest structures, i.e., the hut clusters, should exhibit a significant broadening in reciprocal space due to finite size effects. This broadening is most effective along the vertical momentum transfer $k_\perp$ as the smallest dimension of the huts is their height, as sketched in the inset of Fig. 5(b). For the dome clusters, we expect narrow spots because they exhibit a height which is 3–4 times larger than that of the huts. We therefore assign the broadened Gaussians (blue dotted line in

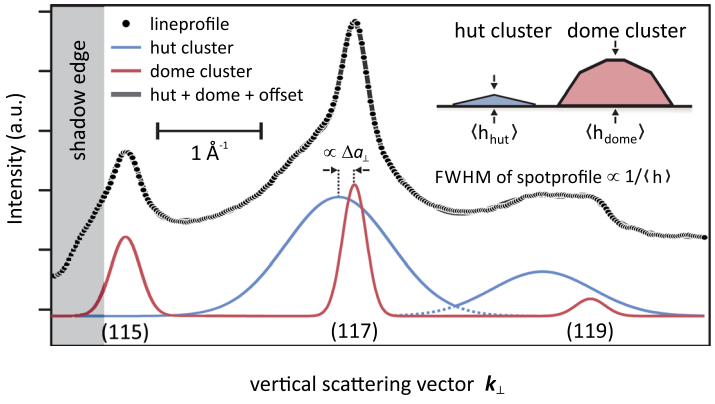

FIG. 4. Line profile of the (117) and (119) spots along $k_\perp$ direction (see also red dashed line in Fig. 3(b)). The profile can be fitted by two broad and narrow Gaussians assigned to diffraction from huts and domes, respectively.

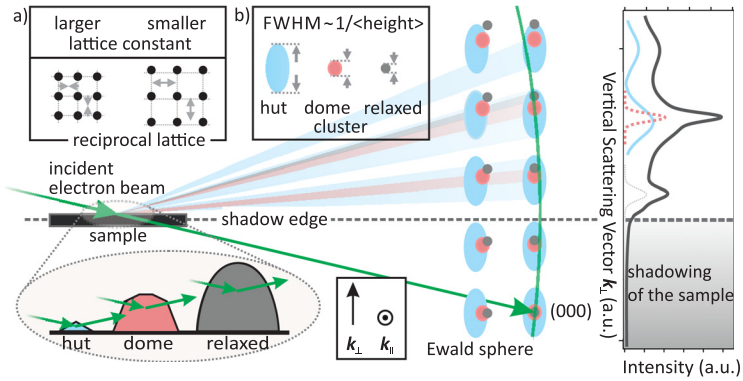

FIG. 5. Sketch of transmission diffraction geometry and Bragg conditions in reciprocal space for hut- (blue), dome- (red), and relaxed clusters (grey). The Ewald sphere is plotted in green. The Bragg conditions are broadened due to finite size effects and are shifted vertically and laterally due to variations of strain state. The spot profile depicts the variation of diffraction intensity along $k_\perp$. For simplicity a simple cubic lattice is used.

Fig. 4) to the 2 nm high hut clusters. The FWHM (full width at half maximum) of $k_\perp = 1.0\,\text{Å}^{-1}$ is slightly larger than the value of $0.62\,\text{Å}^{-1}$, which is expected for diffraction from the entire hut cluster, i.e., assuming infinite mean free path of the electrons, kinematic approximation, and volume weighted hut cluster profile in the direction parallel to the diffraction vector. The narrow Gaussian (red dashed line) originate from the higher and larger dome clusters.

The different strain states of the three cluster types result in slightly different positions of the corresponding diffraction spots. Hut clusters are coherent to the Si substrate and exhibit a 4% increased layer separation by tetragonal distortion.[32] This vertical strain causes a significant shift of the corresponding spots to lower values of $k_\perp$, i.e., towards the (000) Bragg condition or the shadow edge, respectively. From the observed shift $\Delta k_\perp = 0.20\,\text{Å}^{-1}$ of the position of the broad Gaussian to lower values of $\Delta k_\perp$ we conclude an increased layer separation of $\Delta d/d = 2.6\%$ of the hut clusters with respect to the dome clusters. Dome clusters are more relaxed than hut clusters.[32,34] With increasing height to width ratio the strain is more efficiently reduced at the apex of the clusters. We therefore expect a smaller shift of the spot positions for the dome clusters with respect to the spots of the hut clusters. The lateral compression of the hut clusters towards the Si lattice parameter in addition can also be observed through a shift of the spot positions of the broad Gaussian away from the (00) rod to larger values of $k_\parallel$, as sketched in Fig. 5.

Up to now, we have used the width and the position of the diffraction spots to distinguish between contributions from huts and domes. The intensities of these peaks are determined by the dynamical structure factor F_{hkl} and the density of the clusters on the sample, i.e., the diffraction volume, which both are not well defined quantities. Last but not least, also the Laue condition $\Delta\mathbf{k} = \mathbf{G}$ affects the relative intensities and may be used to distinguish between huts and domes. The Laue condition is fulfilled when reciprocal lattice points or lattice rods are intersected by the Ewald sphere, i.e., for spots on the zero order Laue circle or in its direct vicinity as sketched in Fig. 5. In case that the reciprocal lattice points are broadened (due to finite size effects), this condition becomes relaxed. Therefore, diffraction from hut clusters (broad light blue spots in Fig. 5) is still observed for larger vertical momentum transfer, where the dome clusters (light pink spots) no longer contribute to the diffraction pattern because their reciprocal lattice spot is no longer intersected by the Ewald sphere (green line). Such a case is observed for the (119) spot, where the relative intensity of the narrow Gaussian is much smaller than for the (117) spot which is located close to the zero order Laue circle. Thus, all spots on the right hand side of the diffraction pattern arise almost solely from hut clusters.

B. Transient response of the diffraction pattern upon heating

The heating of the Ge clusters upon impulsive fs laser excitation and subsequent cooling to the substrate are determined from the transient intensity drop which is shown in Fig. 6 for different

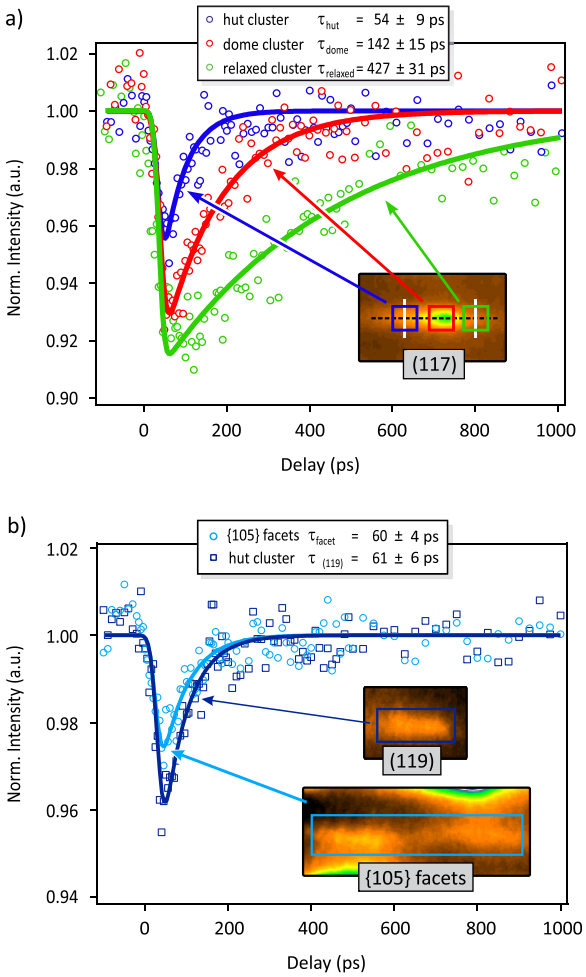

FIG. 6. Transient diffraction intensities as function of time delay Δt (a) different positions of the (117) spot exhibit three different recovery time constants which are assigned to diffraction from hut-, dome-, and relaxed clusters. (b) The transient intensity of the (119) spot and the {105} facet spots originate from hut clusters. Experimental data were fitted by a convolution of monoexponential decay with a temporal response function of 25 ps width.

diffraction spots. The decrease in diffraction signal is related to the Debye-Waller factor D, which is usually written as $D = \exp(-2W)$, where $W = 1/2 \cdot \langle(\mathbf{u} \cdot \mathbf{k})^2\rangle$. Here, $\mathbf{u}$ is the atomic displacement and $\mathbf{k}$ is the momentum transfer of the diffracted electrons. In case of isotropic thermal motion, this expression can be simplified to $W = 1/6 \cdot \mathbf{u}^2\,\mathbf{k}^2$. The atomic displacements $\mathbf{u}$ are composed of contributions from all possible vibrational modes of the system, i.e., acoustic and optical phonons. Applying the Debye model to calculate W for bulk acoustic modes, one obtains[47]

$$W = \frac{3\hbar^2\mathbf{k}^2T}{2Mk_B\Theta_D^2}, \tag{1}$$

where $\Theta_D = 364\,\mathrm{K}$ is the Debye temperature for Ge at 300 K and M is the mass of Ge atoms. The transient intensity drop can be converted into a transient temperature rise using a stationary spot intensity versus sample temperature measurement.[18] Such a calibration procedure gives a precise determination of temperature independent on momentum transfer $\mathbf{k}$ or Debye temperature Θ_D. This calibration also accounts for inherent variations of Θ_D as function of temperature as it is the case for Ge.[48] From our calibration curve, we obtain a Debye temperature of $\Theta_D = 280\,\mathrm{K}$, which is in good agreement with literature values for the temperature regime between 30 and 150 K.[48]

Figure 6(a) shows the transient intensity of the (117) spot as function of time delay Δt between the pump laser pulse and the probe electron pulse. The initial drop at the temporal

overlap $\Delta t = 0$ reflects the heating from 25 K to 150 K upon fs laser excitation which is known to happen on a picosecond timescale.[49] Here, the observed timescale of 25 ps is determined by the temporal response function of the RHEED setup, which is dominated by the so called velocity mismatch between pumping laser pulse and probing electron pulse.[18] The recovery of the spot intensity occurs on a slower timescale and reflects the cooling of the Ge hut clusters through heat transfer to the Si substrate. Applying the above described spot profile analysis, the contributions from hut-, dome-, and relaxed clusters could be discriminated from the profile of the (117) spot. The solid lines are fits to the data assuming an exponential recovery of intensity. We observe three distinct different recovery time constants of $\tau_{\text{hut}} = 54$ ps, $\tau_{\text{dome}} = 140$ ps, and $\tau_{\text{relax}} = 430$ ps, which were assigned to hut-, dome-, and relaxed clusters, respectively.

The results from the transient spot profile analysis are supported by an independent analysis of the (119) spot and the {105} facet spots, which are shown in Fig. 6(b). The intensity of the (119) spot (open squares) is dominated by diffraction from hut clusters and reveals a recovery with $\tau_{(119)} = 61$ ps. The {105} facet spots arise solely from the hut clusters and recover on a timescale of $\tau_{\text{facet}} = 60$ ps. All three recovery time constants for the hut clusters are in good agreement, and we obtain an average cooling time constant of $\tau_{\text{hut}} = 58$ ps.

C. Lifetime map and statistical analysis

The slower recovery time constants for the dome- and relaxed clusters were additionally confirmed by an analysis of the temporal evolution of the entire diffraction pattern, i.e., a so

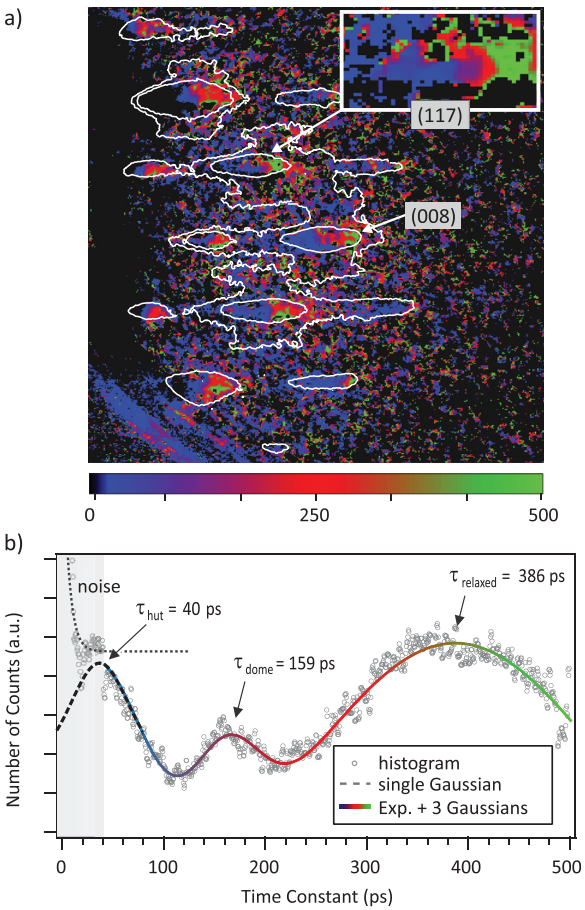

FIG. 7. Pixel by pixel analysis of the entire diffraction pattern, the so called lifetime map. (a) Color separation of diffraction spots indicate different cooling time constants for hut, dome, and relaxed clusters. (b) The histogram of the lifetime map analysis clearly show three distinct cooling time constants, which agree well with the transient spot profile analysis depicted in Fig. 6.

called lifetime map. Each pixel of the temporal series of diffraction patterns is fitted by an exponential recovery function like that used in Fig. 6. Fig. 7(a) displays the recovery time constant using color coding. Blue indicates diffracted intensity with fast recovery time constant up to 100 ps, red—recovery times about 250 ps, while green indicates slow time constant of 400 to 500 ps. Black areas indicate background intensity where the signal to noise ratio was insufficient to provide a proper fit. The blue to red asymmetry of all spots—i.e., blue is on the left, red in the middle, and green is on the right wing of all spots—support the spot profile analysis we have performed before. This is shown more clearly in the inset of Fig. 7(a) showing the (117) spot.

The time constant of all pixels of the diffraction pattern from Fig. 7(a) are sorted in the histogram shown in Fig. 7(b). Three clear maxima can be identified at 40 ps, 160 ps, and 390 ps, which agree well with the recovery time constants for hut-, dome-, and relaxed clusters which were independently determined from the spot profile analysis presented in Fig. 6.

IV. CONCLUSIONS AND SUMMARY

The cooling time constants for the three different cluster types are in qualitative agreement with the theory of nanoscale heat transport in hetero structures: the smallest structure exhibits the shortest cooling time $\tau \propto h/\sigma_{tbc}$ with σ_{tbc} the thermal boundary conductance between Ge and Si. For a more quantitative analysis, temperature dependent numerical simulations of the one dimensional heat diffusion equation were performed.[22,50] The thermal boundary conductance σ_{tbc} was calculated in the framework of the diffuse mismatch model (DMM),[51] including anharmonic inelastic phonon interactions[52] and a real phonon dispersion relation in the [001] crystallographic direction. As the simulations consider a film with uniform thickness h,[50] comparability to the experiment is only provided by calculating the mean height $\langle h \rangle$ of the clusters, i.e., the height of a cylinder with equal volume and base area. Hut clusters are then described by an effective mean height of $\langle h \rangle = 0.8$ nm and dome clusters by $\langle h \rangle = 3.4$ nm. From our simple model, we expect a cooling time constant of 35 ps and 146 ps, respectively, which are in qualitative agreement with the experimental findings. For the large relaxed clusters, an effective mean height cannot be unambiguously specified due to their broadened size distribution.

In summary, we have shown that time-resolved electron diffraction under grazing incidence provides extreme sensitivity even for thinnest films or smallest structures, allowing to study transient processes with nanoscale spatial resolution. Due to the wealth of information in an electron diffraction pattern, i.e., many different spots, spot profiles, and different momentum transfers, it was possible to simultaneously distinguish the ultrafast transient behavior of different nanoscale clusters upon impulsive excitation in one single measurement. Self-organized Ge hut-, dome-, and relaxed clusters were prepared by in-situ deposition on Si(001). These structures were excited by 50 fs laser pulses and thereby heated from a base temperature of 25 K to 150 K. The Debye-Waller effect together with a spot profile analysis and lifetime mapping was employed to follow the cooling dynamics of the three different cluster types. From the transient cooling dynamics upon heating, it was found that the 2.3 nm high hut clusters are cooling with a time constant of $\tau_{\text{hut}} = 58$ ps, while the 6 nm high dome clusters are cooling with $\tau_{\text{dome}} = 154$ ps.

ACKNOWLEDGMENTS

Fruitful discussion with B. Krenzer, F. Klasing, K. Sokolowski-Tinten, and C. Klein and financial support from the Deutsche Forschungsgemeinschaft through SFB616 “Energy dissipation at surfaces” are gratefully acknowledged.

[1]C. W. Siders, A. Cavalleri, K. Sokolowski-Tinten, C. Toth, T. Guo, M. Kammler, M. Horn-von Hoegen, K. R. Wilson, D. von der Linde, and C. P. J. Barty, Science **286**, 1340 (1999).
[2]C. Rose-Petruck, R. Jimenez, T. Guo, A. Cavalleri, C. W. Siders, F. Rksi, J. A. Squier, B. C. Walker, K. R. Wilson, and C. P. J. Barty, Nature **398**, 310 (1999).
[3]K. Sokolowski-Tinten, C. Blome, J. Blums, A. Cavalleri, C. Dietrich, A. Tarasevitch, I. Uschmann, E. Foerster, M. Kammler, M. Horn-von Hoegen, and D. von der Linde, Nature **422**, 287 (2003).
[4]M. Bargheer, N. Zhavoronkov, Y. Gritsai, J. C. Woo, D. S. Kim, M. Woerner, and T. Elsaesser, Science **306**, 1771 (2004).

[5]G. Mourou and S. Williamson, Appl. Phys. Lett. **41**, 44 (1982).
[6]M. Aeschlimann, E. Hull, J. Cao, C. A. Schmuttenmaer, L. G. Jahn, Y. Gao, H. E. Elsayed-Ali, D. A. Mantell, and M. R. Scheinfein, Rev. Sci. Instrum. **66**, 1000 (1995).
[7]B. J. Siwick, J. R. Dwyer, R. E. Jordan, and R. J. D. Miller, Science **302**, 1382 (2003).
[8]C.-Y. Ruan, V. A. Lobastov, F. Vigliotti, S. Chen, and A. H. Zewail, Science **304**, 80 (2004).
[9]S. Nie, X. Wang, H. Park, R. Clinite, and J. Cao, Phys. Rev. Lett. **96**, 025901 (2006).
[10]G. Sciaini, M. Harb, S. G. Kruglik, T. Payer, C. T. Hebeisen, F.-J. Meyer zu Heringdorf, M. Yamaguchi, M. Horn-von Hoegen, R. Ernstorfer, and R. J. D. Miller, Nature **458**, 56 (2009).
[11]M. Eichberger, H. Schäfer, M. Krumova, M. Beyer, J. Demsar, H. Berger, G. Moriena, G. Sciaini, and R. J. D. Miller, Nature **468**, 799 (2010).
[12]M. Gao, C. Lu, H. Jean-Ruel, L. Chung Liu, A. Marx, K. Onda, S. Koshihara, Y. Nakano, X. Shao, T. Hiramatsu, G. Saito, H. Yamochi, R. Cooney, G. Moriena, G. Sciaini, and R. J. D. Miller, Nature **496**, 343 (2013).
[13]D. M. Fritz, D. A. Reis, B. Adams, R. A. Akre, J. Arthur, C. Blome, P. H. Bucksbaum, A. L. Cavalieri, S. Engemann, S. Fahy, R. W. Falcone, P. H. Fuoss, K. J. Gaffney, M. J. George, J. Hajdu, M. P. Hertlein, P. B. Hillyard, M. Horn-von Hoegen, M. Kammler, J. Kaspar, R. Kienberger, P. Krejcik, S. H. Lee, A. M. Lindenberg, B. McFarland, D. Meyer, T. Montagne, E. D. Murray, A. J. Nelson, M. Nicoul, R. Pahl, J. Rudati, H. Schlarb, D. P. Siddons, K. Sokolowski-Tinten, T. Tschentscher, D. von der Linde, and J. B. Hastings, Science **315**, 633 (2007).
[14]R. Ernstorfer, M. Harb, C. T. Hebeisen, G. Sciaini, T. Dartigalongue, and R. J. D. Miller, Science **323**, 1033 (2009).
[15]M. P. Seah and W. A. Dench, Surf. Interface Anal. **1**, 2 (1979).
[16]M. Horn-von Hoegen, Z. Kristallogr. **214**, 684 (1999).
[17]B. Krenzer, A. Janzen, P. Zhou, D. von der Linde, and M. H. von Hoegen, New J. Phys. **8**, 190 (2006).
[18]A. Hanisch-Blicharski, A. Janzen, B. Krenzer, S. Wall, F. Klasing, A. Kalus, T. Frigge, M. Kammler, and M. H. von Hoegen, Ultramicroscopy **127**, 2 (2013).
[19]R. K. Raman, Y. Murooka, C.-Y. Ruan, T. Yang, S. Berber, and D. Tománek, Phys. Rev. Lett. **101**, 077401 (2008).
[20]C.-Y. Ruan, Y. Murooka, R. K. Raman, and R. A. Murdick, Nano Lett. **7**, 1290 (2007).
[21]M. Gulde, S. Schweda, G. Storeck, M. Maiti, H. K. Yu, A. M. Wodtke, S. Schäfer, and C. Ropers, Science **345**, 200 (2014).
[22]T. Frigge, B. Hafke, V. Tinnemann, B. Krenzer, and M. Horn-von Hoegen, Appl. Phys. Lett. **106**, 053108 (2015).
[23]C. A. Paddock and G. L. Eesley, J. Appl. Phys. **60**, 285 (1986).
[24]C. T. D. A. Young and J. Tauc, *Phonon Scattering in Condensed Matter*, edited by A. C. Anderson and J. P. Wolfe (Springer, Berlin, 1986).
[25]E. Bauer, Z. Kristallogr.-Cryst. Mater. **110**, 395 (1958).
[26]Y.-W. Mo, D. E. Savage, B. S. Swartzentruber, and M. G. Lagally, Phys. Rev. Lett. **65**, 1020 (1990).
[27]F. Montalenti, P. Raiteri, D. Migas, H. Von Känel, A. Rastelli, C. Manzano, G. Costantini, U. Denker, O. Schmidt, K. Kern *et al.*, Phys. Rev. Lett. **93**, 216102 (2004).
[28]I. Goldfarb, P. T. Hayden, J. H. G. Owen, and G. A. D. Briggs, Phys. Rev. B **56**, 10459 (1997).
[29]M. Kästner and B. Voigtländer, Phys. Rev. Lett. **82**, 2745 (1999).
[30]G. Medeiros-Ribeiro, A. M. Bratkovski, T. I. Kamins, D. A. A. Ohlberg, and R. S. Williams, Science **279**, 353 (1998).
[31]F. M. Ross, R. M. Tromp, and M. C. Reuter, Science **286**, 1931 (1999).
[32]M. Horn-von Hoegen, B. H. Müller, T. Grabosch, and P. Kury, Phys. Rev. B **70**, 235313 (2004).
[33]A. J. Schell-Sorokin and R. M. Tromp, Phys. Rev. Lett. **64**, 1039 (1990).
[34]G. Wedler, J. Walz, T. Hesjedal, E. Chilla, and R. Koch, Phys. Rev. Lett. **80**, 2382 (1998).
[35]A. J. Steinfort, P. M. L. O. Scholte, A. Ettema, F. Tuinstra, M. Nielsen, E. Landemark, D.-M. Smilgies, R. Feidenhans'l, G. Falkenberg, L. Seehofer, and R. L. Johnson, Phys. Rev. Lett. **77**, 2009 (1996).
[36]D. J. Eaglesham and M. Cerullo, Phys. Rev. Lett. **64**, 1943 (1990).
[37]G. Medeiros-Ribeiro, T. Kamins, D. Ohlberg, and R. S. Williams, Phys. Rev. B **58**, 3533 (1998).
[38]C.-P. Liu, J. M. Gibson, D. G. Cahill, T. I. Kamins, D. P. Basile, and R. S. Williams, Phys. Rev. Lett. **84**, 1958 (2000).
[39]F. Ross, J. Tersoff, and R. Tromp, Phys. Rev. Lett. **80**, 984 (1998).
[40]A. Nikiforov, V. Cherepanov, O. Pchelyakov, A. Dvurechenskii, and A. Yakimov, Thin Solid Films **380**, 158 (2000).
[41]S. Chaparro, Y. Zhang, J. Drucker, D. Chandrasekhar, and D. J. Smith, J. Appl. Phys. **87**, 2245 (2000).
[42]A. Janzen, B. Krenzer, O. Heinz, P. Zhou, D. Thien, A. Hanisch, F.-J. Meyer zu Heringdorf, D. von der Linde, and M. Horn von Hoegen, Rev. Sci. Instrum. **78**, 013906 (2007).
[43]M. Horn-von Hoegen, M. Pook, A. Al Falou, B. H. Müller, and M. Henzler, Surf. Sci. **284**, 53 (1993).
[44]A. Ichimiya and P. I. Cohen, *Reflection High-Energy Electron Diffraction* (Cambridge University Press, 2004).
[45]W. Braun, *Applied RHEED: Reflection High-Energy Electron Diffraction During Crystal Growth*, Springer Tracts in Modern Physics (Springer, 1999).
[46]C. E. Aumann, Y.-W. Mo, and M. G. Lagally, Appl. Phys. Lett. **59**, 1061 (1991).
[47]J. M. Ziman, *Principles of the Theory of Solids* (Cambridge University Press, 1979), p. 64.
[48]P. Flubacher, A. J. Leadbetter, and J. A. Morrison, Philos. Mag. **4**(39), 273 (1959).
[49]K. Sokolowski-Tinten, U. Shymanovich, M. Nicoul, J. Blums, A. Tarasevitch, M. Horn-von Hoegen, D. von der Linde, A. Morak, and T. Wietler, in *Ultrafast Phenomena XV*, Springer Series in Chemical Physics Vol. 88, edited by P. Corkum, D. Jonas, R. Miller, and A. Weiner (Springer Berlin Heidelberg, 2007), pp. 597.
[50]T. Frigge, B. Hafke, V. Tinnemann, T. Witte, B. Krenzer, and M. Horn-von Hoegen, "Nanoscale thermal transport in self-organized epitaxial Ge nanostructures on Si(001)," Semicond. Sci. Technol. (submitted).
[51]E. T. Swartz and R. O. Pohl, Rev. Mod. Phys. **61**, 605 (1989).
[52]T. Beechem, J. C. Duda, P. E. Hopkins, and P. M. Norris, Appl. Phys. Lett. **97**, 061907 (2010).